ACS APPLIED MATERIALS & INTERFACES

Research Article

www.acsami.org

Conductive Upconversion Er,Yb-FTO Nanoparticle Coating To Replace Pt as a Low-Cost and High-Performance Counter Electrode for Dye-Sensitized Solar Cells

Liang Li,[†] Yulin Yang,*[,†] Ruiqing Fan,*[,†] Shuo Chen,[†] Ping Wang,[†] Bin Yang,[‡] and Wenwu Cao*[,‡,§]

[†]Department of Chemistry, Harbin Institute of Technology, Harbin, 150001, People's Republic of China

[‡]Condensed Matter Science and Technology Institute, Harbin Institute of Technology, Harbin, 150080, People's Republic of China

[§]Materials Research Institute, The Pennsylvania State University, University Park, Pennsylvania 16802, United States

Supporting Information

ABSTRACT: F-doped SnO_2 (FTO) nanocrystals modified by Er and Yb with upconversion capability and excellent catalytic properties have been designed and fabricated as an economic replacement for Pt for use as the counter electrode (CE) in dye-sensitized solar cells. The cost of the UC-FTO counter electrode is only $\sim{}^1/_{20}$th of that for Pt. The upconverted luminescence-mediated energy transfer and the superior catalytic property for I_3^-/I^- circulation overpowered the slight degradation caused by increased CE/electrolyte interface resistance. A 23.9% enhancement in photocurrent was achieved with little degradation in photovoltage, resulting in a 9.12% increase in solar-to-electric power conversion efficiency. Near-infrared (NIR) light-to-electricity has been directly observed by SPS and IPCE characterizations, showing the effect of the upconversion counter electrode.

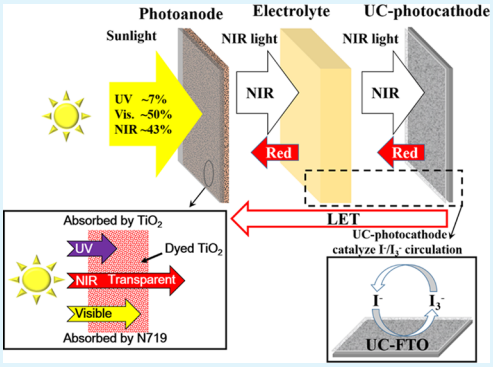

KEYWORDS: *dye-sensitized solar cells, counter electrode, Pt-free, upconversion, conductive, low cost*

INTRODUCTION

Dye-sensitized solar cells (DSSCs) have brought a revolution for photoelectrochemical solar cells, because of their environmental friendliness, simple production processes, low cost, and decent energy conversion efficiency.[1−3] A typical DSSC consists of a dye-sensitized semiconductor electrode, a redox electrolyte, and a counter electrode (CE). The CEs in DSSCs are usually made of platinum, which is one of the world's scarcest noble metals, because of its excellent electrocatalytic activity, high electrical conductivity, and chemical stability.[4,5] Because platinum is the most expensive component in DSSCs,[6] it is highly imperative to develop replacement low-cost CE materials that can function as well as platinum does. Here, we report a new CE material, UC-FTO, whose cost is only ${}^1/_{20}$th of Pt and more importantly, the DSSC fabricated using this new material achieved an overall solar-to-electric power conversion efficiency of 7.30%, which is even better than the 6.69% for the DSSC using platinum as the CE (pt-CE).

Numerous attempts have been made in the past to exploit competent substitutes for Pt in order to reduce the overall cost, while not reduce the overall performance of DSSCs. For example, carbonaceous materials[7−12] and conductive polymers[13,14] have been proposed for use as the CE to replace Pt in DSSCs, but their catalytic activities and stability are less satisfactory. Carbon materials with special size or morphology have been widely studied considering their high electric conductivity, corrosion resistance toward I_2, high reactivity for tri-iodide reduction, and low cost.[15] However, low-cost carbon is worse in power conversion efficiency, compared to Pt-CE. Hard carbon spherule CE for DSSC produced a 5.7% overall power conversion efficiency (PCE), which is slightly less than the 6.5% PCE observed for Pt-CE used for DSSC.[16] Other materials, such as carbon nanotubes[9,17] and graphene,[18−20] were reported to perform much worse than Pt in terms of photovoltaic performance of DSSCs. Although some improvement were made using conductive polymers (e.g., polyaniline,[21] polypyrrole[22]), the increased fabrication cost, low thermal stability, and short lifetime make them less attractive.

Gratzel et al. found that cobalt sulfide has excellent catalytic activity for the iodine-based redox couple,[23] certain inorganic compounds have recently been studied as CE materials for DSSCs, including sulfides,[24−27] nitrides,[4] carbides,[28,29] and oxides.[30,31] Fluorine-doped tin oxide (FTO), which is a low-cost oxide, is an excellent conductive material. SnO_2, which is the base material of FTO, is a good catalyst with excellent chemical stability. Thus, modified FTO possesses the potential to be a low-cost and high-efficiency CE material for DSSCs.

Photons of lower energy, such as near-infrared (NIR) light, cannot be absorbed by the DSSC; hence, they do not contribute to the electrical output. Although many novel dyes

Received: February 16, 2014
Accepted: May 8, 2014
Published: May 8, 2014

with wide absorption spectra have been reported in the literature,[32,33] the high cost, complicated production process, and low yield limited their usage potential in DSSC. A useful method for reducing the transmission loss of lower-energy photons (especially NIR light) is through upconversion (UC), which converts lower-energy photons to higher-energy photons that are in the absorption spectrum of the DSSC, so that the efficiency of solar cells can be increased.[34] Here, we report a successful fabrication of a novel FTO with very low cost ($^1/_{20}$th of the cost of chloroplatinic acid of equal quantity) that has excellent conductivity, decent catalytic properties, and UC capability.

EXPERIMENTAL SECTION

Preparation of UC-FTO. A sample of 15 g of $SnCl_2{\cdot}2H_2O$ with 0.188 g of $Er(NO_3)_3$ and 1.718 g of $Yb(NO_3)_3$ as dopant was dissolved into 50 mL of distilled water. Commercial ammonia then was added into the above solution dropwise, adjusting the pH to 7. The dropping rate must be well-controlled for chemical homogeneity. The product (mainly $Sn(OH)_2$) was washed with distilled water and centrifuged. Aqueous hydrofluoric acid (~1%) was dropped to the above mixture, and a sol–gel mixture of $Sn(OH)_2$ and SnF_2 was obtained. The mixture was transferred into a Teflon-lined stainless-steel vessel, and heated at 200 °C for 24 h after sealing. Then, it was further heated in a muffle in nitrogen at 400 °C for half an hour and natural-cooled to room temperature to produce Er, Yb-FTO nanoscale powder. Slurry of UC-FTO was prepared by mixing UC-FTO and ethyl cellulose in terpinol. Counter electrodes (CEs) were obtained by screen printing on FTO glasses and calcined at 450 °C.

Characterization. Powder X-ray diffraction (XRD) patterns were recorded in the 2θ range of 10°–70° using Cu Kα radiation by Shimadzu Model XRD-6000 X-ray diffractometer. Transmission electron microscopy (TEM) micrographs were taken using FeiTecnia G2-STWIN equipment. The X-ray photoelectron spectroscopy (XPS) result was obtained from a Thermo ESCALAB-250 spectrometer with an Al Kα source, under an ultrahigh vacuum (UHV) at 3.5×10^{-7} Pa. Luminescence spectra and fluorescence lifetimes were measured by the Edinburgh Model FLSP920 combined steady-state fluorescence and phosphorescence lifetime spectrometer, using a 980-nm laser as the excitation source. The SPS instrument was assembled by Jilin University, monochromatic light was obtained by passing light from a 500-W xenon lamp (Beijing Changtuo Co., Model CHF-XQ500W, China) through a double-prism monochromator (Zolix, Model SBP300, China), and the signals were collected by a Stanford Model SR830 DSP lock-in amplifier. IPCE was measured on a Newport EQE/IPCE spectral response system. Electrochemical impedance spectra were recorded using an electrochemical analyzer (Model CHI660D) from Beijing Chenhua Co., China. The sample was sandwiched between two FTO glass electrodes. Optically transparent electrodes were made from an FTO-coated glass plate purchased from Acros Organics, Belgium. The photoanode films were immersed in 0.3 mM N719 (Solaronix SA, Switzerland) in absolute ethyl alcohol for 24 h at room temperature. The electrolyte composed of 0.05 M I_2, 0.5 M LiI, and 0.1 M TBP in 1:1 (volume ratio) acetonitrile–propylene carbonate was admitted by capillary action. Photocurrent–photovoltage curves were recorded using a CH Instruments, Model CHI660D electrochemical analyzer. The light intensity of AM1.5G global sunlight from a filtered 500-W xenon lamp (Newport, Model CHF-XM500, Changtuo, China with an AM1.5G global filter) was calibrated using a standard Si solar cell (calibrated at National Institute of Metrology, PRC). All characterizations were carried out under ambient pressure and temperature.

Based on the photocurrent density–photovoltage (J–V) curve, the fill factor (FF) is defined as

$$\mathrm{FF} = \frac{J_{\max} \times V_{\max}}{J_{SC} \times V_{OC}} \quad (1)$$

where $J_{\max}$ and $V_{\max}$ are the photocurrent density and photovoltage for maximum power output, J_{SC} is the short-circuit photocurrent density, and V_{OC} is the open-circuit photovoltage. The overall power conversion efficiency (PCE) is defined as

$$\mathrm{PCE} = \frac{\mathrm{FF} \times J_{SC} \times V_{OC}}{P_{in}} \quad (2)$$

where P_{in} is the power of incident light, which, in this work, is 100 mW cm^{-2}.

RESULTS AND DISCUSSIONS

The morphology of UC-FTO particles was investigated by TEM, as shown in Figure 1a. The particle size distribution is

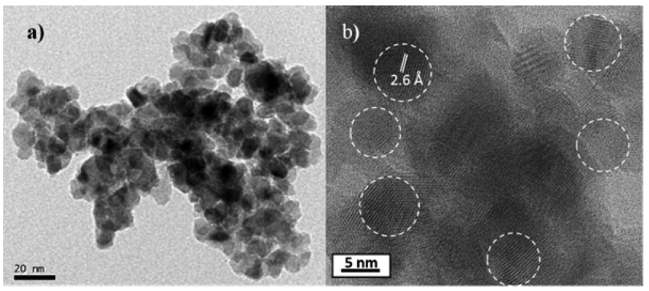

Figure 1. TEM images of UC-FTO nanoparticles with lattice fringes.

~7–8 nm and the as-prepared nanoparticles are single domain crystallites (Figure 1b). The interplanar spacing of d_{101} derived from the lattice fringes are 2.6 Å, which is in good agreement with the theoretical values (d_{101} = 2.64 Å). The crystal phase was confirmed through XRD pattern (see Figure S1 in the Supporting Information). To investigate the composition of UC-FTO nanoparticles, XPS, EDS, and element distribution mapping were carried out (see Figures S2 and S3 in the Supporting Information for details).

Figure 2a shows the luminescence emission spectra of UC-FTO nanoparticles under 980-nm laser excitation with different pump powers. The photoluminescence spectrum exhibits three

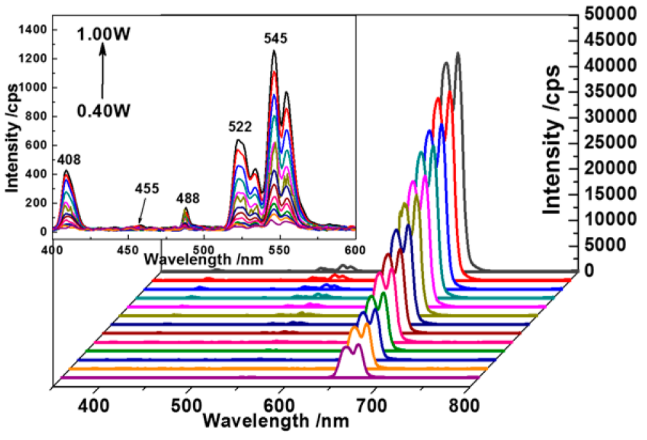

Figure 2. UC luminesce spectra of UC-FTO with different pump power ranging from 0.40 W to 1.00 W under 980-nm excitation. (Magnifying spectra from 300 nm to 600 nm are shown as the inset. Peaks centered at 522, 545, and 660 nm correspond to Er^{3+}:$^2H_{11/2} \rightarrow {}^4I_{15/2}$, $^4S_{3/2} \rightarrow {}^4I_{15/2}$, and $^4F_{9/2} \rightarrow {}^4I_{15/2}$ transitions, and the peak at 660 nm is the strongest peak. Peaks centered at 408, 455, and 488 nm correspond to Er^{3+}:$^2H_{9/2} \rightarrow {}^4I_{15/2}$, $^4F_{5/2} \rightarrow {}^4I_{15/2}$, and $^4F_{7/2} \rightarrow {}^4I_{15/2}$ transitions, respectively.)

dx.doi.org/10.1021/am5009776 | ACS Appl. Mater. Interfaces 2014, 6, 8223–8229

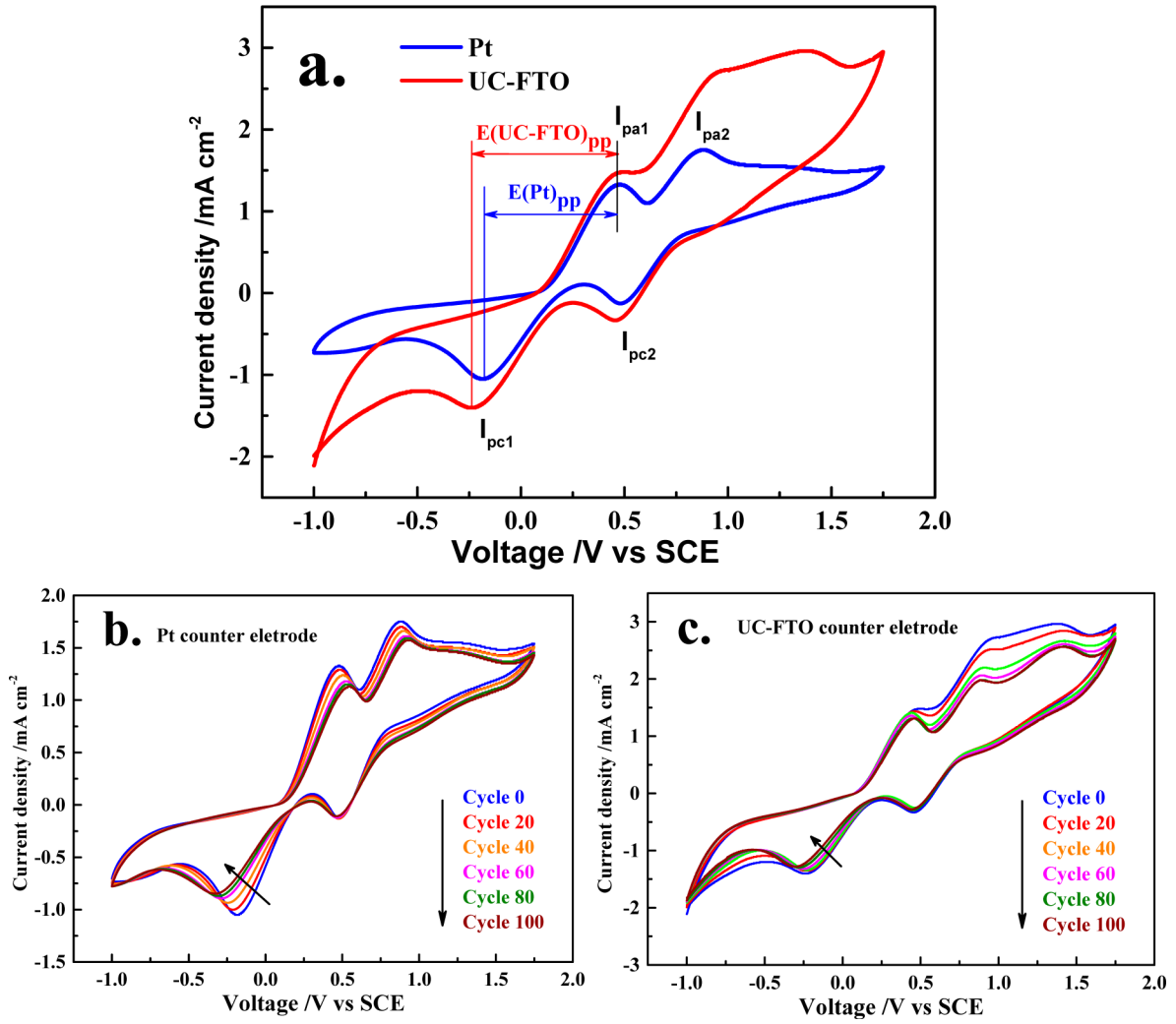

Figure 3. Cyclic voltammograms for Pt and UC-FTO electrodes in 0.01 M LiI, 0.001 M I_2, and 0.1 M $LiClO_4$ acetonitrile solutions at a scan rate of 50 mV s^{-1}: (a) CVs for Pt and UC-FTO electrodes; (b) 100 consecutive CVs for Pt-CE; and (c) 100 consecutive CVs for UC-FTO-CE.

distinct Er^{3+} emission bands, weak in green and much stronger in red. The peaks centered at 522, 545, and 660 nm correspond to Er^{3+}:$^2H_{11/2} \rightarrow {}^4I_{15/2}$, $^4S_{3/2} \rightarrow {}^4I_{15/2}$, and $^4F_{9/2} \rightarrow {}^4I_{15/2}$ transitions, respectively.[35,36] Taking the peak at 660 nm as an example, the intensity increases with the laser power, following the relationship of $I_{UC} \propto P^n$,[37,38] where n is the pump photons required to excite rare-earth (RE) ions from the ground state to the emitting excited state. The n values for 660 and 545 nm are 2.02 and 2.20, respectively; both n values correspond to the two-photon process (confirmed by Figure S4 in the Supporting Information). Figure 2b shows the enlarged luminescence emission spectra of UC-FTO from 400 nm to 600 nm. The peaks centered at 408, 455, and 488 nm correspond to Er^{3+}:$^2H_{9/2} \rightarrow {}^4I_{15/2}$, $^4F_{5/2} \rightarrow {}^4I_{15/2}$, and $^4F_{7/2} \rightarrow {}^4I_{15/2}$ transitions, respectively. The possible mechanism of the UC process is discussed in the Supporting Information (see Figure S5).

The catalytic properties and reaction kinetics of the UC-FTO and Pt electrodes were investigated simultaneously by cyclic voltammetric (CV) measurements, and the results are plotted in Figure 3a. Similar to the Pt electrode,[23] for the UC-FTO electrode, there exist two anodic current peaks (I_{pa1}: $3I^- = I_3^- + 2e^-$, and I_{pa2}: $2I_3^- = 3I_2 + 2e^-$) and two cathodic current peaks (I_{pc1}: $I_3^- + 2e^- = 3I^-$, and I_{pc2}: $3I_2 + 2e^- = 2I_3^-$).[39−41] Here, we focus on peaks I_{pa1} and I_{pc1}, since the CE is responsible for the reduction of I_3^- in DSSCs. The result indicated that the electrolyte of I^-/I_3^- can circulate on either surface of the Pt or UC-FTO electrodes. The peak-to-peak separation (E_{pp}) and peak current density, which is negatively correlated with the standard electrochemical rate constant of a redox reaction, are two critical parameters used to quantify electrocatalytic activities of different CEs.[42] The E_{pp} value in the UC-FTO (705 mV) is close to that in Pt (643 mV), indicating a total reserve of high reversibility of I_3^-/I^- circulation in Pt CE. Furthermore, the UC-FTO CE has even higher redox peaks toward I_3^-/I^- catalysis, indicating its superior catalytic ability, relative to Pt-CE. In general, smaller size nanoparticle UC-FTO layer provides larger interfacial surface area with I^-/I_3^- redox electrolyte, resulting in increased catalytic activity. The enhanced electrocatalytic activity can be attributed to its higher specific surface and more rapid electron transfer nature from the FTO, and the intrinsically excellent electrocatalytic activity after doping with Er and Yb. In addition, the diffusion coefficient (D_n) in the Randles−Sevcik equation is proportional to the peak current density:[43]

$$i_p = Kn_{e^{1.5}}AD^{0.5}c\upsilon^{0.5} \quad (3)$$

where $K = 2.69 \times 10^5$ is a constant, n_e is the number of electrodes contributing to the charge transfer, A is the electrode

dx.doi.org/10.1021/am5009776 | ACS Appl. Mater. Interfaces 2014, 6, 8223−8229

area, c represents the bulk concentration of I_3^- species, D is the diffusivity, and υ is the scanning rate. The diffusivity in the UC-FTO CE is 5.51×10^{-6} cm^{-2} s^{-1}, which is 82% larger than that in the Pt CE (3.02×10^{-6} cm^{-2} s^{-1}), presumably arising from its ultrasmall nanostructure, along with a greatly increased active surface area.

Figures 3b and 3c show 100 successive CV cycles of Pt-CE and UC-FTO-CE, respectively. In the consecutive 100 CV tests, the CVs change little. All redox peak current densities of UC-FTO-CE retain stable with increasing the cycle number, which is similar to Pt-CE. This indicates that UC-FTO has good chemical stability and is tightly bound to the FTO glass surface for the same composition.

As shown in Figure 4, there are mainly three parts in a DSSC: a photoanode, an electrolyte, and a UC-photocathode.

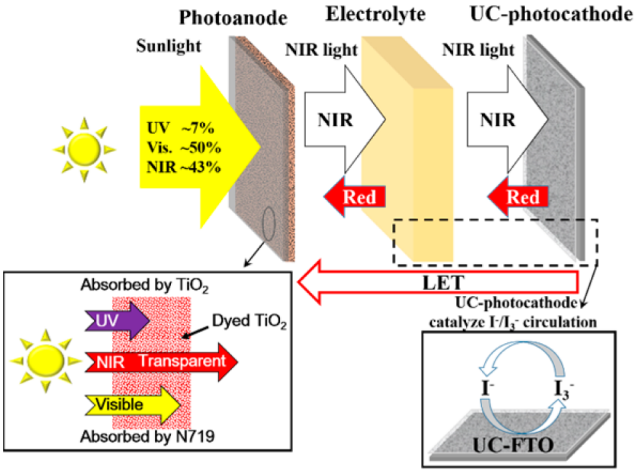

Figure 4. Illustration of the photon process of a working dye-sensitized solar cell (DSSC) with a UC-FTO photocathode.

In the sun radiation energy distribution, there is ~7% ultraviolet light, ~50% visible light, and ~43% NIR light. When sunlight goes through the photoanode, the UV light is absorbed by the TiO_2 and visible light is absorbed by N719, which is coated on the surface of TiO_2 nanoparticles. The UC-photocathode is excited by the NIR light and then emits red light by the UC-FTO. Finally, the upconverted red light reflected from the CE excites N719 from the reverse direction. In addition, the UC-photocathode can catalyze I^-/I_3^- circulation and accelerate I^- regeneration, to increase the concentration of I^- with reducibility.

The electron-process in DSSC with UC-FTO is illustrated in Figure 5. Under the illumination of sunlight, the Dye goes to the excited state (Dye*) and injects one electron into the conductive band of TiO_2 for each excited-dye molecule. Dye* loses one electron and becomes oxidized Dye^+. The injected electrons diffuse into the external circuit and finally into the back contact. To regenerate free-state Dye, I^- ions in electrolyte reduce Dye^+ back to Dye, while itself becomes oxidized I_3^-. The number of I_3^- can be reduced by electrons from the back contact. UC-FTO can catalyze this process, resulting in the increase of I^- in the electrolyte.

While pursuing photovoltaic efficiency in the NIR region, it is important to maintain the overall performance of solar cells. In order to study the effect of UC nanocrystals on the overall performance of solar cells, surface photovoltage (SPV) responses of cells using Pt or UC-FTO were tested as CEs,

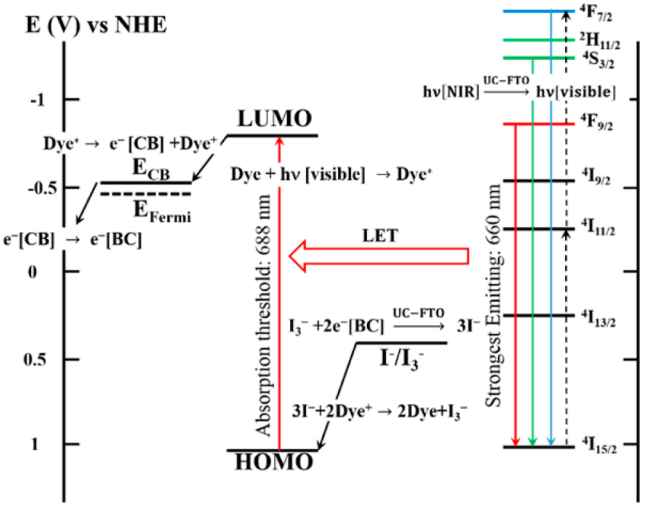

Figure 5. Electron process of a working DSSC with a UC-FTO photocathode.

and the results are shown in Figure 6. Both DSSCs utilized commercial P25 as photoanodes. The SPV analysis for UC-

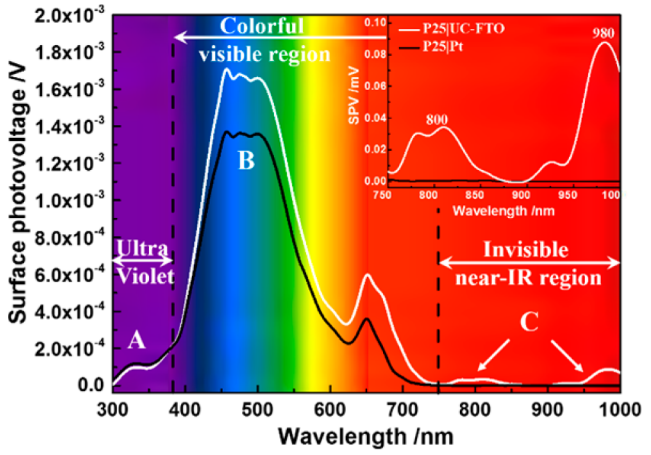

Figure 6. Surface photovoltage (SPV) spectra of a DSSC with Pt or UC-FTO as the counter electrode from 300−1000 nm. Inset highlights the near-infrared (NIR) region.

FTO samples demonstrates three characteristic response peaks in the entire spectrum of sunlight from 300 nm to 1000 nm, which are marked as peaks A, B, and C, respectively. In the ultraviolet (UV) region, a typical characteristic response peak from 300−380 nm (peak A) can be assigned to the band−band electronic transition in TiO_2. For the same photoanode, the two samples showed almost the same level response in the UV region. The broad peak from 400 nm to 700 nm can be assigned to the dye sensitization of N719. Compared with cells using Pt, an overall increasing intensity of peak B was found in cells using UC-FTO, which indicates an enhanced circulation of I^-/I_3^-. More newly born I^- can efficiently and rapidly regenerate oxidized dye molecules, which help improve the SPV response and enhance the conversion efficiency of DSSCs. In addition, a new band of response appeared in the NIR region from 750 nm to 1000 nm (peak C), which confirmed the effect and LET mechanism of upconversion. The two NIR responses correspond to Er:$^4I_{9/2}$ and Er:$^4I_{11/2}$ and Yb:$^2F_{5/2}$. NIR light of

dx.doi.org/10.1021/am5009776 | ACS Appl. Mater. Interfaces 2014, 6, 8223−8229

~800−980 nm can be absorbed by UC-FTO nanoparticles, which emit visible light and are being utilized.

Photocurrent density−voltage (J−V) curves under simulated solar light irradiation of 100 mW cm^{-2} (AM1.5G global) are shown in Figure 7 for DSSCs using CEs made of UC-FTO and

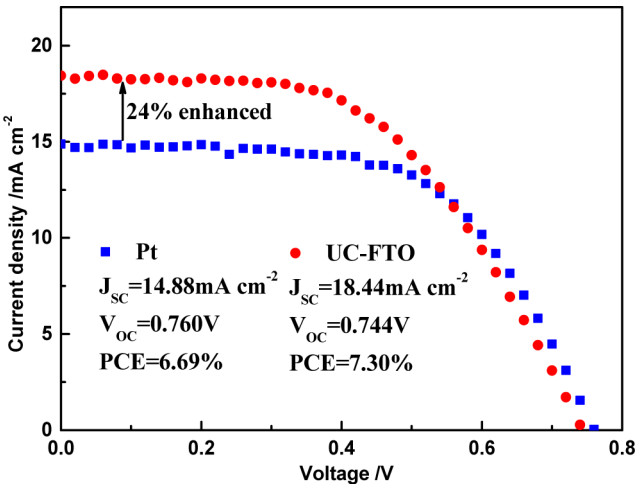

Figure 7. Photocurrent density−voltage (J−V) curves of DSSCs with UC-FTO or Pt.

Pt. For reproducibility, each value for cell performance was an average result from three samples. The photocurrent density of DSSC using UC-FTO CE is J = 18.44 mA cm^{-2}, which is a 23.9% increase, compared with the photocurrent density of 14.88 mA cm^{-2} from a DSSC using Pt CE. The voltage value of DSSC with UP-FTO maintained 97.89% of that of DSSC with Pt, which is 0.744 V, while the total performance PCE value increased from 6.69% to 7.30%. More importantly, the cost of UC-FTO is only ~$^1/_{20}$th of that for Pt (an equivalent amount of Pt contained in chloroplatinic acid, see Table S2 in the Supporting Information for details).

As can be seen in the incident photon to current (IPCE) spectra (Figure 8), the photon-to-current conversion efficiency obviously increased in the visible region. This indicates that the UC-FTO nanoparticles enhanced the catalytic performance of the electrolyte, which produced better circulation of I^-/I_3^-, hence, enhancing the conversion efficiency of DSSCs. Besides

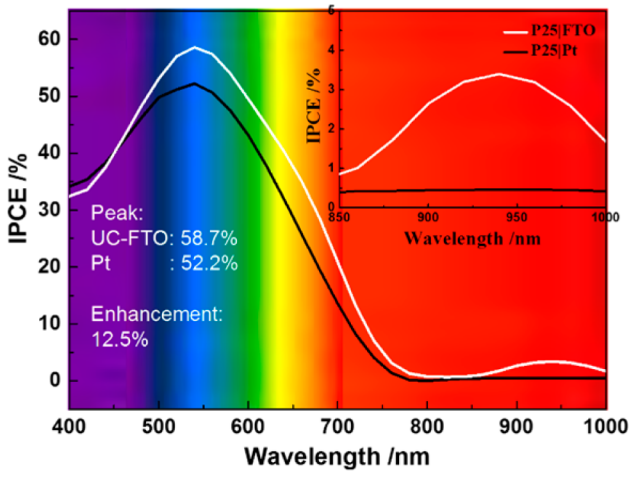

Figure 8. IPCE curves of solar cells with Pt or UC-FTO as the CE.

the enhanced visible IPCE, a small peak in the NIR region can be found in Figure 8.

Electric impedance spectra (EIS) is a powerful method for investigating internal resistance that is attributed to the charge-transfer properties of DSSCs. Impedance at low frequencies (0.05−1 Hz) corresponds to the Nernst diffusion of I_3^-/I^- within the electrolyte. The capacitance and charge-transfer resistance at the CE|I_3^-/I^- electrolyte interface are associated with impedance at higher frequencies (1−100 kHz). The response in the range of 1−100 Hz corresponds to the dyed-$TiO_2|I_3^-/I^-$ electrolyte interface.[44] Figure S6 in the Supporting Information shows the EIS of DSSCs with UC-FTO and Pt as CE materials. The sinusoidal perturbation was set to −0.8 V. Table S1 in the Supporting Information summarizes parameters of the equivalent circuit $R_S[C_1(R_1O_1)](R_2Q_1)$, and the results are discussed in detail in the Supporting Information.

CONCLUSIONS

In summary, a conducive layer made of upconverted fluorine-doped tin oxide (UC-FTO) nanoparticles was successfully synthesized, which has good conductivity, decent catalytic properties, and the capability to upconvert near-infrared (NIR) light to visible light, to increase the total efficiency of solar cells. It can substantially reduce the cost of the counter electrode (CE) by replacing the expensive platinum (~$^1/_{20}$th of that for Pt). By using this novel material as the CE in dye-sensitized solar cells (DSSCs), the overall power conversion efficiency (PCE) of the DSSC was increased to 7.30%, which represents an enhancement of more than 9.12%, compared with DSSC using a platinum counter electrode (denoted as Pt-CE; 6.69%). To date, this is the only known material that not only substantially reduced the cost of the CE, but also effectively increased the overall performance of DSSCs. Our results suggest a promising strategy of using conductive upconversion materials as the CE to further reduce the cost and simultaneously enhance the overall efficiency of solar cells.

ASSOCIATED CONTENT

Supporting Information

XRD and XPS of UC-FTO samples. Details concerning the UC process and mechanism. EIS and cost summary of DSSCs. This material is available free of charge via the Internet at http://pubs.acs.org.

AUTHOR INFORMATION

Corresponding Authors

*Tel.: +86 451 86413710. Fax: +86 451 86418270. E-mail: ylyang@hit.edu.cn (Y. L. Yang).

*Tel.: +86 451 86413710. Fax: +86 451 86418270. E-mail: fanruiqing@hit.edu.cn (R. Q. Fan).

*Tel.: +1 814 8654101. Fax: +1 814 8652326. E-mail: dzk@psu.edu (W. W. Cao).

Notes

The authors declare no competing financial interest.

ACKNOWLEDGMENTS

This work was supported by National Natural Science Foundation of China (Grant Nos. 21171044 and 21371040) and the National Key Basic Research Program of China (973 Program, No. 2013CB632900). The work was also supported by the Fundamental Research Funds for the Central Universities (Grant No. HIT. IBRSEM. A. 201409), Program

for Innovation Research of Science in Harbin Institute of Technology (PIRS of HIT No.A201416 and B201414), and National Key Technology Research and Development Program of China No. 2013BAI03B06.

REFERENCES

(1) Oregan, B.; Gratzel, M. A Low-Cost, High-Efficiency Solar-Cell Based on Dye-Sensitized Colloidal TiO_2 Films. *Nature* **1991**, *353*, 737−740.
(2) Gratzel, M. Photoelectrochemical cells. *Nature* **2001**, *414*, 338−344.
(3) Gong, F.; Wang, H.; Xu, X.; Zhou, G.; Wang, Z. S. In Situ Growth of $Co_{0.85}Se$ and $Ni_{0.85}Se$ on Conductive Substrates as High-Performance Counter Electrodes for Dye-Sensitized Solar Cells. *J. Am. Chem. Soc.* **2012**, *134*, 10953−10958.
(4) Jiang, Q. W.; Li, G. R.; Gao, X. P. Highly Ordered TiN Nanotube Arrays as Counter Electrodes for Dye-sensitized Solar Cells. *Chem. Commun.* **2009**, 6720−6722.
(5) Papageorgiou, N.; Maier, W. F.; Gratzel, M. An Iodine/Triiodide Reduction Electrocatalyst for Aqueous and Organic Media. *J. Electrochem. Soc.* **1997**, *144*, 876−884.
(6) Smestad, G.; Bignozzi, C.; Argazzi, R. Testing of Dye-Sensitized TiO_2 Solar-Cells.1. Experimental Photocurrent Output and Conversion Efficiencies. *Sol. Energy Mater. Sol. Cells* **1994**, *32*, 259−272.
(7) Lee, K. S.; Lee, W. J.; Park, N. G.; Kim, S. O.; Park, J. H. Transferred Vertically Aligned N-Doped Carbon Nanotube Arrays: Use in Dye-Sensitized Solar Cells as Counter Electrodes. *Chem. Commun.* **2011**, *47*, 4264−4266.
(8) Murakami, T. N.; Ito, S.; Wang, Q.; Nazeeruddin, M. K.; Bessho, T.; Cesar, I.; Liska, P.; Humphry-Baker, R.; Comte, P.; Pechy, P.; Gratzel, M. Highly Efficient Dye-sensitized Solar Cells Based on Carbon Black Counter Electrodes. *J. Electrochem. Soc.* **2006**, *153*, A2255−A2261.
(9) Han, J.; Kim, H.; Kim, D. Y.; Jo, S. M.; Jang, S. Y. Water-Soluble Polyelectrolyte-Grafted Multiwalled Carbon Nanotube Thin Films for Efficient Counter Electrode of Dye-Sensitized Solar Cells. *ACS Nano* **2010**, *4*, 3503−3509.
(10) Kavan, L.; Yum, J. H.; Gratzel, M. Optically Transparent Cathode for Dye-Sensitized Solar Cells Based on Graphene Nanoplatelets. *ACS Nano* **2011**, *5*, 165−172.
(11) Velten, J.; Mozer, A. J.; Li, D.; Officer, D.; Wallace, G.; Baughman, R.; Zakhidov, A. Carbon Nanotube/Graphene Nanocomposite as Efficient Counter Electrodes in Dye-Sensitized Solar Cells. *Nanotechnology* **2012**, *23*, 085201−1∼6.
(12) Xue, Y. H.; Liu, J.; Chen, H.; Wang, R. G.; Li, D. Q.; Qu, J.; Dai, L. M. Nitrogen-Doped Graphene Foams as Metal-Free Counter Electrodes in High-Performance Dye-Sensitized Solar Cells. *Angew. Chem., Int. Ed.* **2012**, *51*, 12124−12127.
(13) Xia, J. B.; Masaki, N.; Jiang, K. J.; Yanagida, S. The Influence of Doping Ions on Poly(3,4-Ethylenedioxythiophene) as a Counter Electrode of a Dye-Sensitized Solar Cell. *J. Mater. Chem.* **2007**, *17*, 2845−2850.
(14) Ameen, S.; Akhtar, M. S.; Kim, Y. S.; Yang, O. B.; Shin, H. S. Sulfamic Acid-Doped Polyaniline Nanofibers Thin Film-Based Counter Electrode: Application in Dye-Sensitized Solar Cells. *J. Phys. Chem. C* **2010**, *114*, 4760−4764.
(15) Kay, A.; Gratzel, M. Low Cost Photovoltaic Modules Based on Dye Sensitized Nanocrystalline Titanium Dioxide and Carbon Powder. *Sol. Energy Mater. Sol. Cells* **1996**, *44*, 99−117.
(16) Huang, Z.; Liu, X. H.; Li, K. X.; Li, D. M.; Luo, Y. H.; Li, H.; Song, W. B.; Chen, L. Q.; Meng, Q. B. Application of Carbon Materials as Counter Electrodes of Dye-Sensitized Solar Cells. *Electrochem. Commun.* **2007**, *9*, 596−598.
(17) Cha, S. I.; Koo, B. K.; Seo, S. H.; Lee, D. Y. Pt-free Transparent Counter Electrodes for Dye-sensitized Solar Cells Prepared from Carbon Nanotube Micro-balls. *J. Mater. Chem.* **2010**, *20*, 659−662.
(18) Choi, H.; Kim, H.; Hwang, S.; Han, Y.; Jeon, M. Graphene Counter Electrodes for Dye-Sensitized Solar Cells Prepared by Electrophoretic Deposition. *J. Mater. Chem.* **2011**, *21*, 7548−7551.
(19) Sahoo, N. G.; Pan, Y. Z.; Li, L.; Chan, S. H. Graphene-Based Materials for Energy Conversion. *Adv. Mater.* **2012**, *24*, 4203−4210.
(20) Huang, X.; Zeng, Z. Y.; Fan, Z. X.; Liu, J. Q.; Zhang, H. Graphene-Based Electrodes. *Adv. Mater.* **2012**, *24*, 5979−6004.
(21) Li, Q. H.; Wu, J. H.; Tang, Q. W.; Lan, Z.; Li, P. J.; Lin, J. M.; Fan, L. Q. Application of Microporous Polyaniline Counter Electrode for Dye-sensitized Solar Cells. *Electrochem. Commun.* **2008**, *10*, 1299−1302.
(22) Wu, J. H.; Li, Q. H.; Fan, L. Q.; Lan, Z.; Li, P. J.; Lin, J. M.; Hao, S. C. High-Performance Polypyrrole Nanoparticles Counter Electrode for Dye-Sensitized Solar Cells. *J. Power Sources* **2008**, *181*, 172−176.
(23) Wang, M. K.; Anghel, A. M.; Marsan, B.; Ha, N. L. C.; Pootrakulchote, N.; Zakeeruddin, S. M.; Gratzel, M. CoS Supersedes Pt as Efficient Electrocatalyst for Triiodide Reduction in Dye-Sensitized Solar Cells. *J. Am. Chem. Soc.* **2009**, *131*, 15976−15977.
(24) Xin, X. K.; He, M.; Han, W.; Jung, J. H.; Lin, Z. Q. Low-Cost Copper Zinc Tin Sulfide Counter Electrodes for High-Efficiency Dye-Sensitized Solar Cells. *Angew. Chem., Int. Ed.* **2011**, *50*, 11739−11742.
(25) Kung, C. W.; Chen, H. W.; Lin, C. Y.; Huang, K. C.; Vittal, R.; Ho, K. C. CoS Acicular Nanorod Arrays for the Counter Electrode of an Efficient Dye-Sensitized Solar Cell. *ACS Nano* **2012**, *6*, 7016−7025.
(26) Sun, H. C.; Qin, D.; Huang, S. Q.; Guo, X. Z.; Li, D. M.; Luo, Y. H.; Meng, Q. B. Dye-sensitized Solar Cells with NiS Counter Electrodes Electrodeposited by a Potential Reversal Technique. *Energy Environ. Sci.* **2011**, *4*, 2630−2637.
(27) Wu, M. X.; Wang, Y. D.; Lin, X.; Yu, N. S.; Wang, L.; Wang, L. L.; Hagfeldt, A.; Ma, T. L. Economical and Effective Sulfide Catalysts for Dye-Sensitized Solar Cells as Counter Electrodes. *Phys. Chem. Chem. Phys.* **2011**, *13*, 19298−19301.
(28) Jang, J. S.; Ham, D. J.; Ramasamy, E.; Lee, J.; Lee, J. S. Platinum-Free Tungsten Carbides as an Efficient Counter Electrode for Dye Sensitized Solar Cells. *Chem. Commun.* **2010**, *46*, 8600−8602.
(29) Wu, M. X.; Lin, X. A.; Hagfeldt, A.; Ma, T. L. Low-Cost Molybdenum Carbide and Tungsten Carbide Counter Electrodes for Dye-Sensitized Solar Cells. *Angew. Chem., Int. Ed.* **2011**, *50*, 3520−3524.
(30) Wu, M. X.; Lin, X. A.; Hagfeldt, A.; Ma, T. L. A Novel Catalyst of WO_2 Nanorod for the Counter Electrode of Dye-Sensitized Solar Cells. *Chem. Commun.* **2011**, *47*, 4535−4537.
(31) Lin, X.; Wu, M. X.; Wang, Y. D.; Hagfeldt, A.; Ma, T. L. Novel Counter Electrode Catalysts of Niobium Oxides Supersede Pt for Dye-Sensitized Solar Cells. *Chem. Commun.* **2011**, *47*, 11489−11491.
(32) Hara, K.; Sato, T.; Katoh, R.; Furube, A.; Ohga, Y.; Shinpo, A.; Suga, S.; Sayama, K.; Sugihara, H.; Arakawa, H. Molecular Design of Coumarin Dyes for Efficient Dye-Sensitized Solar Cells. *J. Phys. Chem. B* **2003**, *107*, 597−606.
(33) Campbell, W. M.; Burrell, A. K.; Officer, D. L.; Jolley, K. W. Porphyrins as Light Harvesters in the Dye-sensitized TiO_2 Solar Cell. *Coordin. Chem. Rev.* **2004**, *248*, 1363−1379.
(34) Yuan, C. Z.; Chen, G. Y.; Prasad, P. N.; Ohulchanskyy, T. Y.; Ning, Z. J.; Tian, H. N.; Sun, L. C.; Agren, H. Use of Colloidal Upconversion Nanocrystals for Energy Relay Solar Cell Light Harvesting in the Near-Infrared Region. *J. Mater. Chem.* **2012**, *22*, 16709−16713.
(35) Budijono, S. J.; Shan, J. N.; Yao, N.; Miura, Y.; Hoye, T.; Austin, R. H.; Ju, Y. G.; Prud'homme, R. K. Synthesis of Stable Block-Copolymer-Protected $NaYF_4:Yb^{3+}$, Er^{3+} Up-Converting Phosphor Nanoparticles. *Chem. Mater.* **2010**, *22*, 311−318.
(36) Matsuura, D.; Ikeuchi, T.; Soga, K. Upconversion Luminescence of Colloidal Solution of Y_2O_3 Nano-Particles Doped with Trivalent Rare-Earth Ions. *J. Lumin.* **2008**, *128*, 1267−1270.
(37) Liang, X. F.; Huang, X. Y.; Zhang, Q. Y. $Gd_2(MoO_4)_3:Er^{3+}$ Nanophosphors for an Enhancement of Silicon Solar-Cell Near-Infrared Response. *J. Fluoresc.* **2009**, *19*, 285−289.
(38) Moadhen, A.; Bouzidi, C.; Elhouichet, H.; Chtourou, R.; Oueslati, M. Concentration and Temperature Dependence of Visible

Up-conversion Luminescence in Sol−Gel SnO_2 Doped with Erbium. *Opt. Mater.* **2009**, *31*, 1224−1227.
(39) Lee, K. M.; Chen, P. Y.; Hsu, C. Y.; Huang, J. H.; Ho, W. H.; Chen, H. C.; Ho, K. C. A High-Performance Counter Electrode Based on Poly(3,4-alkylenedioxythiophene) for Dye-Sensitized Solar Cells. *J. Power Sources* **2009**, *188*, 313−318.
(40) Balamurugan, J.; Thangamuthu, R.; Pandurangan, A.; Jayachandran, M. Facile Fabrication of Dye-Sensitized Solar Cells Utilizing Carbon Nanotubes Grown over 2D Hexagonal Bimetallic Ordered Mesoporous Materials. *J. Power Sources* **2013**, *225*, 364−373.
(41) Luo, J.; Niu, H. J.; Wu, W. J.; Wang, C.; Bai, X. D.; Wang, W. Enhancement of the Efficiency of Dye-Sensitized Solar Cell with Multi-wall Carbon Nanotubes/Polythiophene Composite Counter Electrodes Prepared by Electrodeposition. *Solid State Sci.* **2012**, *14*, 145−149.
(42) Roy-Mayhew, J. D.; Bozym, D. J.; Punckt, C.; Aksay, I. A. Functionalized Graphene as a Catalytic Counter Electrode in Dye-Sensitized Solar Cells. *ACS Nano* **2010**, *4*, 6203−6211.
(43) Xiao, Y. M.; Lin, J. Y.; Wu, J. H.; Tai, S. Y.; Yue, G. T. Pulse Potentiostatic Electropolymerization of High Performance PEDOT Counter Electrodes for Pt-Free Dye-Sensitized Solar Cells. *Electrochim. Acta* **2012**, *83*, 221−226.
(44) Li, Y.; Wang, G. F.; Pan, K.; Jiang, B. J.; Tian, C. G.; Zhou, W.; Fu, H. G. $NaYF_4$:Er^{3+}/Yb^{3+}-Graphene Composites: Preparation, Upconversion Luminescence, and Application in Dye-Sensitized Solar Cells. *J. Mater. Chem.* **2012**, *22*, 20381−20386.